PE&RS
Photogrammetric Engineering Remote Sensing

Volume LV May 1989 Number 5 Part 1

PE&RS
Photogrammetric Engineering & Remote Sensing (ISSN 0099-1112) is published monthly by the American Society for Photogrammetry and Remote Sensing, 210 Little Falls St., Falls Church, VA 22046. Second-class postage paid at Falls Church, Virginia and at additional mailing offices.

SUBSCRIPTIONS
Subscription rate for nonmembers is $110.00 per calendar year (add $20.00 for international subscriptions). Membership dues include annual subscription to *PE&RS* ($24 members and $11 student member). This subscription price is part of membership benefits and cannot be deducted from annual dues. Foreign Airmail subscription is $190.00; US First Class Mail subscription is $140.00. POSTMASTER: Send address changes to *PE&RS*, ASPRS Headquarters, 210 Little Falls St., Falls Church, VA 22046.

MEMBERSHIP
Membership in the Society is open to any person actively engaged in the practice of photogrammetry, photointerpretation, remote sensing, and geographic information systems; or who by means of education or profession is interested in the application or development of these arts and sciences. The annual dues for Regular members are $45.00 Annual dues for accredited Student members are $18.00. Add $15.00 for all international memberships to cover cost of postage. (All memberships are on a calendar year basis.)
Printed in the United States of America.

Fractal Analysis of a Classified Landsat Scene

Lee De Cola
Department of Geography, University of Vermont, Burlington, VT 05405

ABSTRACT: Remotely sensed images tend to be spatially very complicated, revealing regions of homogeneously classified pixels with quite convoluted perimeters. Fractal analysis, the study of complicated phenomena manifesting self-similarity at many scales, is suited to the description of the form and sizes of these regions. I apply fractal analysis to the patterns created by eight land-cover classes from a Landsat TM image of northwest Vermont. The results suggest that forests manifest high fractal dimension and large regions, agricultural activities have large regions with fractal dimension inversely related to the intensity of cultivation, and urban land cover yields small regions with relatively high fractal dimension. Analysis of the individual urban regions provides a data structure in the form of a raster-based GIS which can be used to investigate the location and description of individual regions and to diagnose the reliability of the classification and labeling processes.

INTRODUCTION

THE OBJECTIVE OF THIS PAPER is to demonstrate the applicability of fractal concepts to the spatial analysis of classified digital imagery. The paper is organized as follows. In the next section I use an example of an ideal fractal process to illustrate the theory underlying the analytical technique to be developed. Next, I introduce an algorithmic approach to three analytical steps: the segmentation of a classified image into homogeneous regions, the estimation for each class of the fractal dimension of regional perimeters, and the determination of a parameter describing regional sizes. Section four presents the empirical analysis of the eight land-cover classes from a Landsat Thematic Mapper image of northwest Vermont. This discussion provides fractal parameters which can be related to the classes, as well as a database containing locations and descriptions of the individual regions (clusters of pixels) from each class. I conclude by outlining a complete image segmentation/fractal analysis/GIS scheme that could profit from such advanced computing techniques as parallel processing.

FRACTALS AND REMOTE SENSING

REGIONS IN THE SPATIAL ANALYSIS OF DIGITAL DATA

The processing of digital image sensed data relies heavily on the analysis of energy spectra in order to classify pixels and to make judgments about the appropriateness of class labels. A great deal of attention in the literature is therefore given to quite sophisticated multidimensional techniques for the examination of patterns in the *spectral* space spanned by the various sensor bands (Richards, 1986). The pattern recognition literature, however, concentrates more on the investigation of the *spatial* patterns made by the classes themselves in the Euclidean space ($\mathcal{R}^2$ or the real plane) in which the image lies (NASA, 1988, chapter 7). This distinction is not meant to deny the existence in remote sensing analysis of such approaches as filtering and fourier techniques, which examine both neighborhood patterns at the small scale as well as texture and orientation characteristics at the large (Whalley and Orford, 1982). But it must be admitted that comparatively little use is made of much of the rich information that can be extracted from the spatial as opposed to the spectral characteristics of a scene.

An important reason for the relatively restricted extent of explicitly spatial techniques is the daunting complexity and apparent noisiness of images. Figure 1, for example, shows the patterns made by each of the eight classes of 256^2 pixels centered around St Albans, Vermont (these images are subscenes from the full study area discussed below). The human eye has little trouble distinguishing among the various textures, shapes, and forms in these pictures; yet it is at present a major challenge to bestow even rudimentary visual sophistication upon machines (Hillis, 1985). The first characteristic to appreciate about such patterns, however, is that they are formed of a collection of distinct regions of different sizes and circumscribed by complicated perimeters of various lengths. Let us focus, therefore, on the numbers, sizes, and perimeters of regions formed by clusters of homogeneous pixels in the digital (or map) space $I \times I = I^2$ (a subset of $\mathcal{R}^2$).

THE FRACTAL DIMENSION OF REGIONAL PERIMETERS

A fractal has been defined recently by Benoit Mandelbrot as a pattern "made of parts similar to the whole in some way" (quoted in Feder (1988), p. 11). Phenomena displaying apparent self-similarity are abundant in the real world. Observation reveals that large waves are made up of smaller waves and ripples, clouds can be decomposed into smaller clouds and wisps, trees are made up of hierarchical systems of trunks-branches-twigs-leaves-veins, and so forth. Current fractal research in the spatial sciences makes use of the fact that complicatedness is a direct consequence of the operation of many different spatial processes at a wide range of scales. Mark and Aronson (1984), for example, use fractal dimension to describe terrains; Arlinghaus (1985) demonstrates the fractal nature of central place systems; and Plotnick (1986) points out the fractal characteristics of sedimentation.

In what follows I shall explore the application of fractal concepts to regions, which may be defined as connected sets of points, e.g., pixel locations, for which area is an appropriate measure. A natural way to describe and compare regions is by measuring area, which in the case of a digital image would be a count of the number of pixels in the region multiplied by the area of each pixel. Another regional characteristic is shape, which may be defined as the degree of similarity between the region and some simple geometric figure. Indices of shape have a venerable geographic history (Haggett *et al.*, 1977, section 9.6), but shape is by no means a simple concept. For digital spatial data the concept of shape requires a measurement of regional perimeter, which may be defined as the number of line segments bounding the region.

A common example of the investigation of regions is the fractal analysis of islands and continents, which are bounded by coastlines having a fractal dimension D, defined below (Mandelbrot, 1982, chapter 5). In fact, a coastline is simply one kind of perimeter — in this case an isoline at sea level — having fractal dimension ranging from $D = 1$ (a straight line) to $D = 2$ (an infinitely complicated and therefore plane-filling curve) (Goodchild and Dubuc, 1987; Burrough, 1986). When the scale of analysis is increased, coastlines reveal three important and

PHOTOGRAMMETRIC ENGINEERING AND REMOTE SENSING,
Vol. 55, No. 5, May 1989, pp. 601–610.

0099-1112/89/5505–601$02.25/0

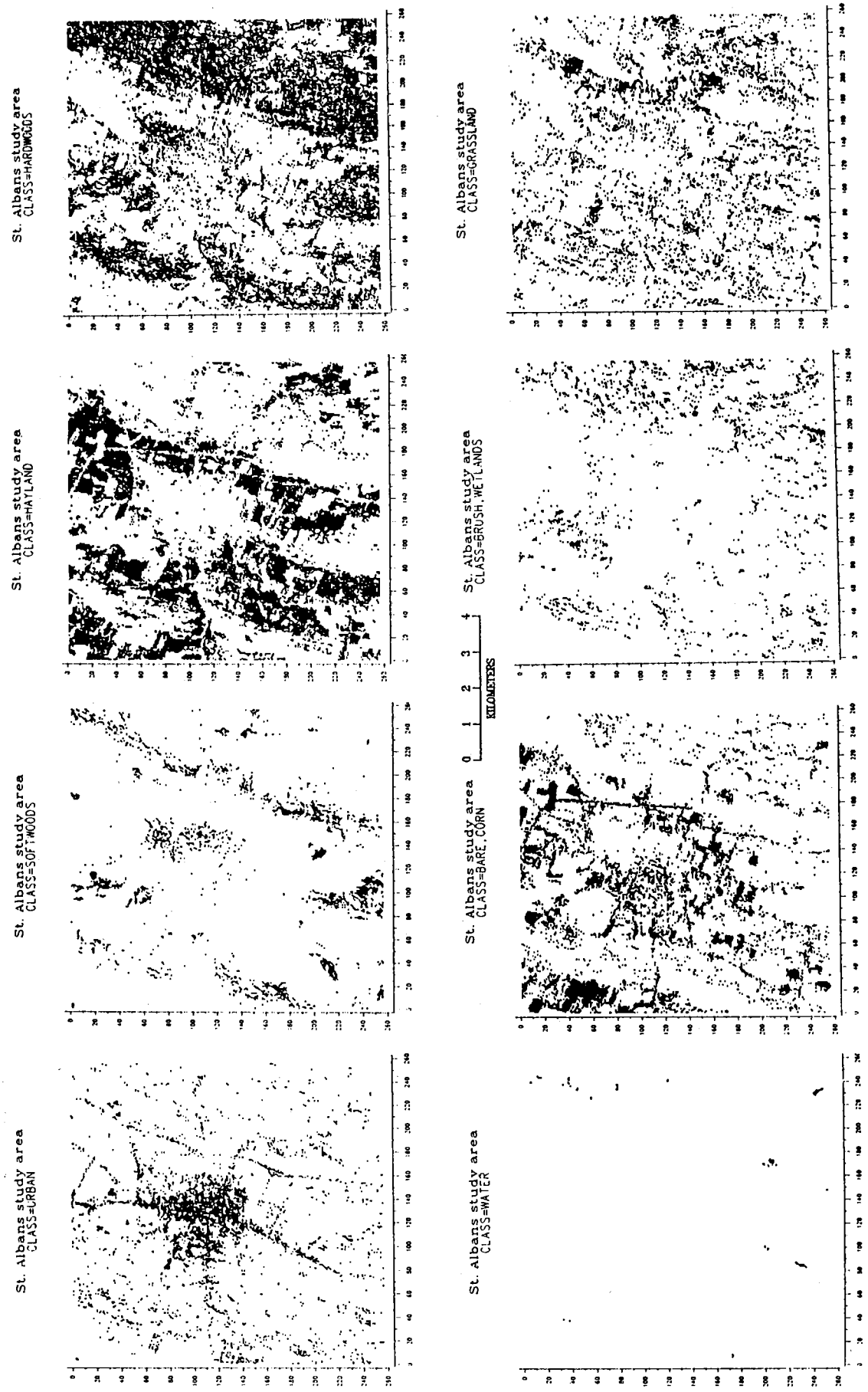

FIG. 1. Regions generated by eight land-cover classes in a 256- by 256-pixel window around St Albans, Vermont, from the full study area.

related characteristics. First, as Mandelbrot observes above, these curves are self-similar: large scale patterns look very much like small scale patterns. Second, these curves are quite complicated, so that lengths measured at large scales are greater than lengths measured at small scales. Third, these regions tend to have no characteristic size. I shall discuss this third characteristic below.

Consider for the moment the two sets of regions shown in Figure 2: squares and so-called Koch quadratic figure (Mandelbrot, 1982, chapter 12; Feder, 1988, chapter 12). These "regions" may be measured in terms of AREA and PERIMETER.On the one hand, note that for squares -- regions with smooth perimeters -- it is the case that PERIMETER $\propto \sqrt{\text{AREA}^1}$. This relationship holds for all regions of fractal dimension $D = 1$, and for squares in particular it is the case that PERIMETER $= 4\sqrt{\text{AREA}^1}$.

Now consider, on the other hand, the Koch quadratic regions, which have been constructed to have the same AREAs as the squares — 16 and 256, respectively — but with significantly more convoluted perimeters, so that PERIMETER $\propto \sqrt{\text{AREA}^{3/2}}$. Consequently, large Koch regions reveal more detail than do small regions, even though the former are constructed from the latter. In other words, if we think of the larger figures as "growing" out of the smaller figures (perhaps as a specific type of land cover spreads), then for the Koch model perimeter grows faster than it does in the case of growing squares. In fact, these Koch regions have been constructed with PERIMETER $= 4\sqrt{\text{AREA}^{3/2}}$.

To make this argument more formal, for any region let $s =$ AREA (or, more generally, "size") and $p =$ PERIMETER. If a given region is bounded by a *smooth* perimeter of fractal dimension $D = 1$, then it is the case that

$$p = c\sqrt{s} \tag{1}$$

where $c = 4$ for a square, $c = 2\sqrt{\pi}$ for a disk, and so forth. In such cases — where we assume that any imaging system of however small a resolution would continue to show a smooth perimeter — c is an index of shape.

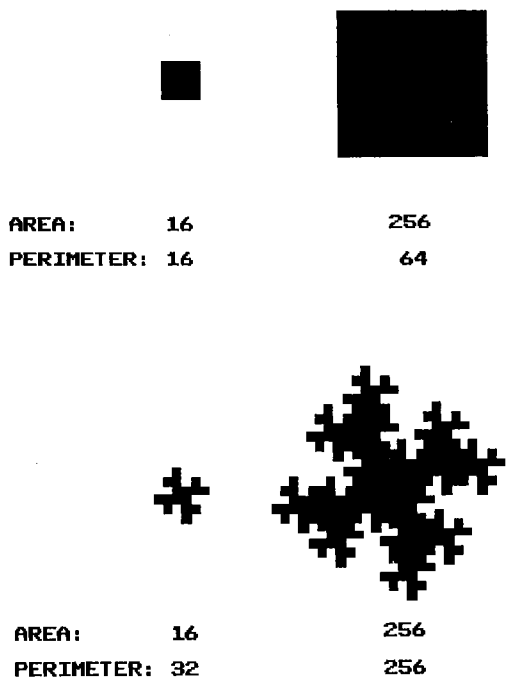

FIG. 2. Comparisons of measurements of squares ($D = 1$) and Koch regions ($D = 3/2$).

For a *fractal* phenomenon, however, it is the case that

$$p = c\sqrt{s}^D \tag{2}$$

where $1 \leq D \leq 2$. For smooth shapes such as circles and squares (which might be called "degenerate" fractals) $D = 1$, as in Equation 1, while $D = 3/2$ for the Koch model, and $D = 2$ in the case of infinitely complicated feature whose perimeter fills the plane. Mandelbrot (1982, chapter 12) uses the term "fractal dimension" to characterize the parameter D.

It should be emphasized that two spatial indices are therefore being distinguished here: c, a measure of overall regional *shape* (which, because $c = 4$ in both cases, obviously does *not* distinguish between the square and the Koch regions!) and fractal dimension D, an index of what I call regional *form* or perimeter complicatedness. The Koch model illustrates the essential self-similarity of ideal fractals: each increase in map scale (in this case by a linear factor of 4) reveals a longer perimeter (here by a factor of $(4)^{3/2} = 8$) in the case of complicated figures than in the case of simple figures. In other words, fractal phenomena for which $D > 1$ have the cartographically commonplace characteristic of revealing more detail at a larger scale. Moreover, at a *given* scale, larger features manifest significantly longer perimeters (by the exponent D) than do smaller. It is these inter-feature comparisons of area and perimeter that I shall use below to estimate regional fractal dimension D according to Equation 2.

TECHNIQUE

Image Segmentation and the Creation of Regions

Perhaps the clearest empirical example of the kind of argument to be used here is Lovejoy's (1982) fractal analysis of cloud images. Clouds tend to be quite complicated, self-similar phenomena. Lovejoy studied digital Geostationary Operational Environmental Satellite (GOES) and radar images of clouds and rain areas using the perimeter/area relationship of Equation 2 and determined that the fractal dimension of the perimeter of these cloud/regions was $D = 1.73$ over a range of cloud sizes from less than 1 km^2 to over 10^6 km^2. Lovejoy's technique is formalized in this section and applied below to the analysis of land-cover classes from a Thematic Mapper image.

Let a digital space be $I^2 = I \times I$, where I is the set of integers, and let $W \subset I^2$ be a square image or "window" composed of N^2 pixels $x \in W$. Next, associate with each of these pixels an integer-valued index $i \in [0, m] \subset I$ representing one of m land cover classes (class 0 can be regarded as residual or unclassified). In the simplest case $m = 1$ so that the image is a black-and-white scene such as the 6 by 6 image shown in Figure 3; class 0 is colored white and class 1 colored black.

Each class i, therefore, imposes a *regionalization* on the image corresponding to the $m+1$-valued function f: $x \rightarrow [0, m]$. For any i a subset of this regionalization is the set $F_i = \{x: f(x) = i\}$, the set of all pixels to which the class i is ascribed. The first step in image description is usually the examination of the set $\{N_i\}$, the histogram of the image given by the number of pixels in each class i, and the corresponding fraction of such pixels $\{f_i\}$, where $f_i = N_i/N_i^2$. For the simple scene, $f_1 = 9/36$.

Labeling may be thought of as the association of some spatial/spectral pattern with class i, but for the moment assume that the pixels are merely assigned to distinct categories: spectral, functional, or otherwise. Let us therefore focus on a single land-cover class and, for convenience, drop references to the index i. We shall return later to inter-class comparisons, once class i has been spatially characterized.

The following image segmentation algorithm partitions the regionalization F (referred to as F_i above) into n distinct and disjoint *regions* E_j such that $\cup E_j = F$, where $j = 1, \ldots, n$. Each

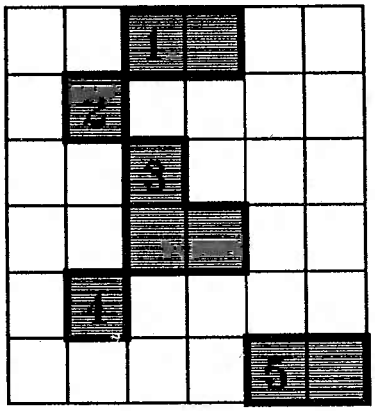

FIG. 3. A simple 6 by 6 two-class image with five regions.

region is grown using the recursive "rook's" rule that for any $x \in E_j$ then $y \in E_j$ if both $f(y) = i$ (the class index) and x and y are either row or column adjacent, i.e., y is a north, south, east, or west neighbor of x (Rosenfeld and Kak, 1982). In the present case I begin at x, the upper left pixel (leftmost pixel of uppermost row) of region E_j, and then recursively add pixels y to the set, sweeping down the image and across each row until all adjacent pixels have been accounted for. Note that the pixel x may be used to stand for unique location, which is of value in associating the region with some geographic feature such as place, link, physical region, etc.

Figure 3 illustrates this approach, providing $n = 5$ distinct regions for the 6×6 simple image. The algorithm produces a set of regions $\{E_j: j = 1, \ldots, n\}$ in which each E_j is a distinct "island" such that, for any $k \neq j$, E_j and E_k are not only disjoint (they share no pixels) but also unconnected (they share no edge). Obviously, the number of regions n is an important descriptor of the regionalization F.

Description of the Regions

Having identified the unique collection of pixels associated with each region E_j, we next determine the area and perimeter of each region. In the case of a specific imaging system, the area of each pixel (the instantaneous field-of-view of the delivered data product) may be standardized to unity. Then let the *area* or size of any region E_j be s_j, the number of pixels in the region. Next, the perimeter of a region E_j is a subset of the edges of its constituent pixels. Consider two adjacent pixels x and y and define a unit of perimeter to exist when $f(x) \neq f(y)$: pixels x and y are obviously not in the same region; therefore, an "active" edge exists between them. Let the *perimeter* p_j of region j be the number of active pixel edges bounding the region. For example, for a single-pixel region $p = 4$, while a one-class image will have a single region for which $p = 4N$. In the case of the simple image of Figure 3, E_3 is the largest region, $s_3 = 3$, and $p_3 = 8$: i.e.,

REGION j	ROW	COLUMN	AREA s_j	PERIMETER p_j
1	1	3	2	6
2	2	2	1	4
3	3	3	3	8
4	5	2	1	4
5	6	5	2	6

Fractal Analysis of Regional Perimeters

Following from the discussion in the previous section, if we assume that digital regions, like the Koch regions of Figure 2, have fractal characteristics over a wide range of scales, then it is possible to determine D for the collection of regions $\{E_j\}$ associated with a given class. The two parameters from Equation 2 may be estimated from the linear expression

$$\ln(p_j) = \ln(c) + D \ln(\sqrt{s_j}) + \epsilon \tag{3}$$

where ϵ is an error term reflecting the homogeneity of the regions as well as the consistency of the classification process. This equation yields D for a specific class. I focus on D and not c becuase the former should reflect spatial pattern, in the sense that land covers having smooth perimeters should have $D \sim 1$ and covers with complicated perimeters should have $D > 1$. Two further details should be noted here. First, natural logarithms will be used in the analysis for computational speed: Figure 4 shows the natural logarithm of regional perimeter plotted against the log of regional area, as well as the regression line, for regions from the URBAN class in the Landsat image discussed below. Second, as in all regression modeling, residuals estimating ϵ will be useful in describing observations (the n regions) and diagnosing the effectiveness of the regression model (Equation 3).

Pareto Analysis of Regional Size

Fractal analysis therefore provides a practical measure of the forms of regions generated by classification, but what of the sizes or areas of these regions $\{s_j\}$? In addition to self-similarity, another important characteristic of fractal phenomena is *scaling*, or the tendency of sets of fractals to have no characteristic or typical size (Feder, 1988, chapter 2). For fractal regions in particular, this means that increasing the size of a window W is likely to bring into view a larger region, while decreasing pixel size (or increasing the number of pixels in a given window) will always reveal smaller regions. The phenomenon of scaling allows us to describe the size distribution of regions.

Let the regions be ordered from largest to smallest by area s, and define rank

$$r_j = Nr(E{:}s > s_j) + 1 \tag{4}$$

which is the number of regions larger than E_j. One statistic characterizing $\{s_j\}$ is the median $\tilde{s} = \{s: r_j = n/2\}$. But a typical problem with digital images is that $\tilde{s} = 1$ in many cases — i.e.,

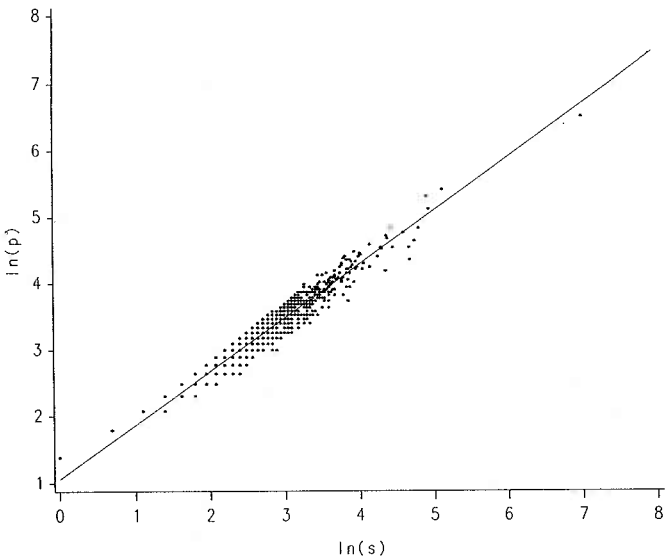

FIG. 4. Plot of natural logarithm of PERIMETER$_j$ by natural logarithm of AREA$_j$ for the URBAN class, with regression line.

more than half the regions are single pixels — so clearly $\bar{s}$ is likely to have little descriptive value.

Another way to characterize the size distribution of the n regions is max$\{s_j\}$, the size of the region of rank $r_j = 1$, which statistic may be descriptive of the underlying pattern but obviously will be strongly determined as well by the specific window W chosen. A more effective tactic is to use the hyperbolic form of Equation 4, reflecting the size distribution of $\{s\}$, to examine the Pareto function describing the sizes of the regions from their unique ranks (Goodchild and Mark, 1987; De Cola, in press).

To do this, we capitalize on a consequence of scaling: that the largest region in W generally bears the same relationship in size to the next largest region as the 10th largest region does to the 20th: i.e., ratios of ranks tend to be similar to some power of the inverse ratios of sizes. More generally, this gives a hyperbolic relationship

$$s_j = A(r_j)^{-b} \tag{5}$$

whose parameters may be estimated from the linear model

$$\ln(s_j) = \ln(A) - b \ln(r_j) + \epsilon \tag{6}$$

which provides least-squares estimates both of the size parameter $a = \ln(A)$ (a prediction of max$\{s_j\}$) as well as of b, the Pareto index of inequality. The Pareto parameter a is a convenient measure of the size of the regions $\{E_j\}$ and less sensitive (more statistically robust) than max$\{s_j\}$. (See De Cola (1985) for empirical results from a rank-size analysis of city populations, and Arnold (1983, pp. 44, 202) for the details of the technique as well as the properties of the estimators.)

It should be noted that the regression Equation 6 is fitted to unique size groups rather than to each region; this avoids the problem of estimating a line through data which are heavily dominated by small (single- or few-pixel) regions, so that we are able to describe the larger regions of inherently greater interest. Figure 5 illustrates the data and regression line for the URBAN class from the Landsat image discussed below.

Spatial Statistics Describing Classes

We now have an ensemble of six spatial statistics describing the image W. Spectral image classification produces $i = 1, \ldots, m$ classes, which can be described in terms of both (1) the number of pixels N_i and (2) the fraction f_i of the scene classified in class i. Image segmentation provides information about (3) the number of connected regions n_i and (4) the size of the largest region max $\{s\}_i$. Finally, fractal analysis yields (5) fractal dimension D_i and (6) the Pareto size parameter a_i reflecting the areas of the regions generated by class i.

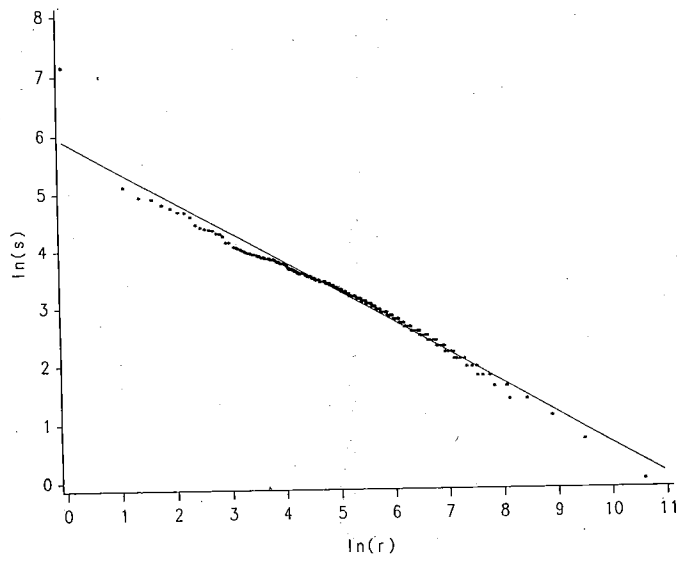

FIG. 5. Plot of natural logarithm of $AREA_j$ by natural logarithm of $RANK_j$ for the URBAN class, with regression line.

ANALYSIS OF THE LANDSAT IMAGE

The Northwest Vermont Study Area

The methodology described above was applied to a 26 October 1982 Landsat Thematic Mapper image of a 4200 km^2 area of northwest Vermont (Figure 6). The data, consisting of 2048^2 pixels each of size (31.81 m)^2, were geometrically corrected and subjected to supervised classification using the Interactive Digital Image Manipulation System (IDIMS) at the NASA Goddard Space Flight Center. Eight land-cover classes were ultimately created, shown in Plate 1. The image is spatially quite complicated, yet the analytical system outlined above is able to resolve this spatial pattern into distinct regional measurements.

Description of the Regions

Table 1 presents the ensemble of key indices for each of the eight land-cover classes in the image. The 3.7 million pixels of

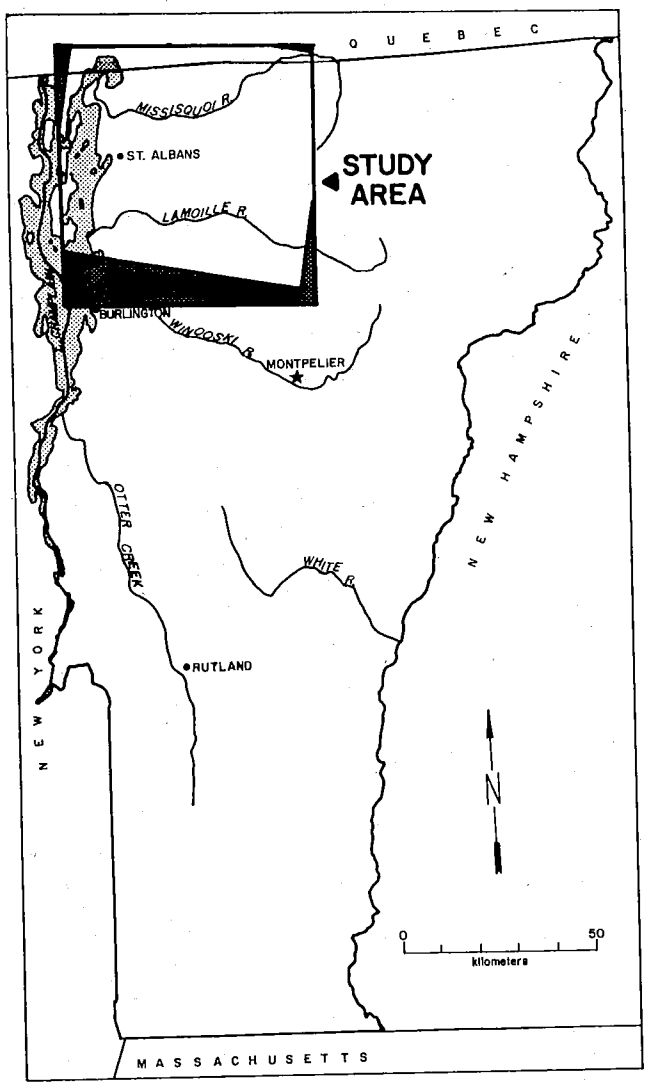

FIG. 6. Location of the classified Landsat TM scene.

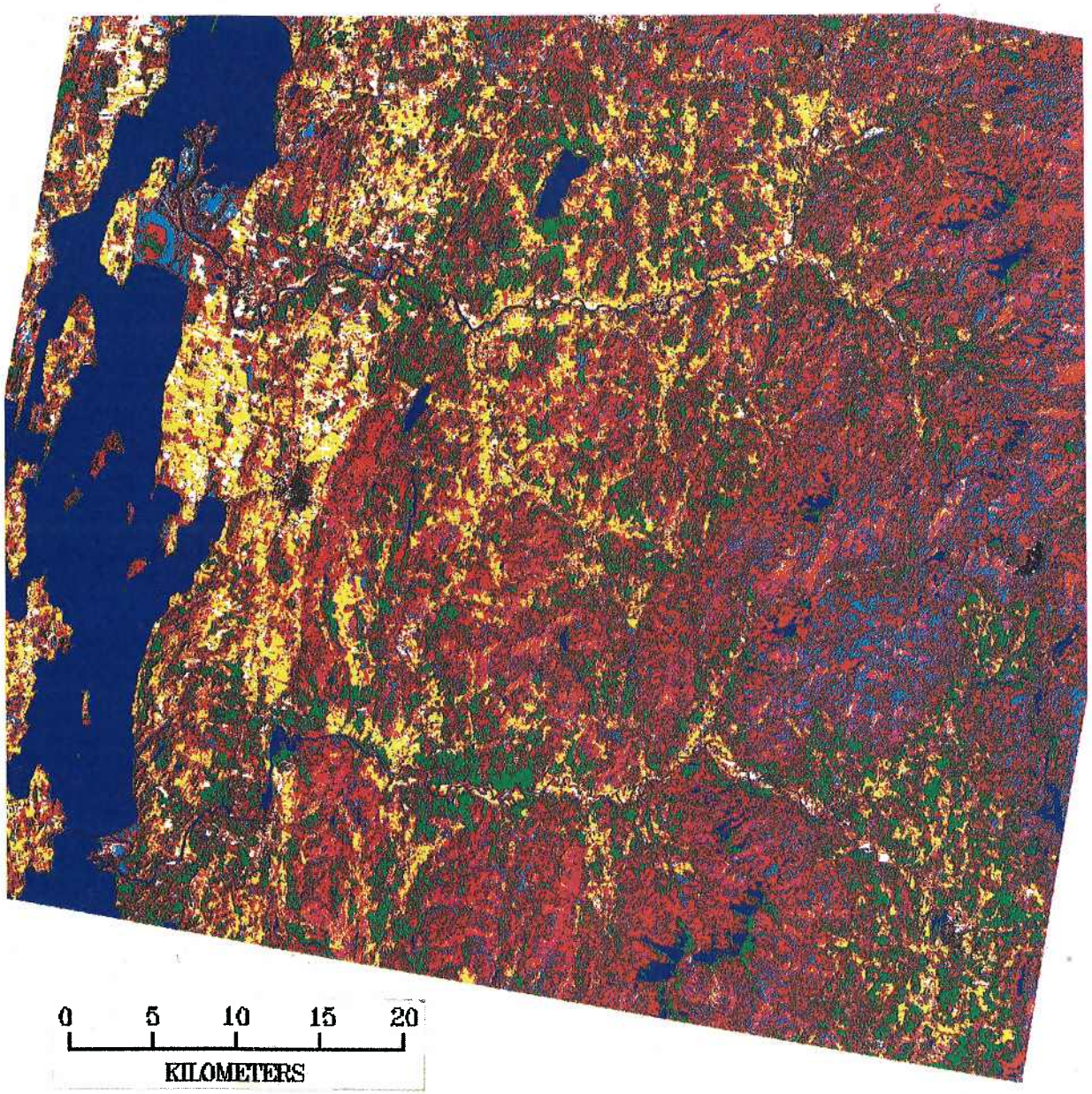

PLATE 1. Classified Landsat TM image for northwest Vermont.

the image have been aggregated into 480,000 regions whose number, size, and form describe the land-cover classes. Almost 40 percent of the pixels in the scene (but only 13 percent of the regions) are classified as HARDWOODS, largely representing the maple forests associated with much of the Vermont landscape. The HAYLAND class constitutes the second dominant land cover, which along with SOFTWOODS and HARDWOODS account for over 72 percent of the dry land cover in the scene. At the other